Production of $O_2(^1\Delta)$ in flowing plasmas using spiker-sustainer excitation

Natalia Y. Babaeva[a)]
Department of Electrical and Computer Engineering, Iowa State University, Ames, Iowa 50011

Ramesh A. Arakoni[b)]
Department of Aerospace Engineering, University of Illinois, Urbana, Illinois 61801

Mark J. Kushner[c)]
Department of Electrical and Computer Engineering, Iowa State University, Ames, Iowa 50011

(Received 3 December 2005; accepted 2 March 2006; published online 9 June 2006)

In chemical oxygen iodine lasers (COILs), oscillation at 1.315 μm in atomic iodine ($^2P_{1/2} \rightarrow {}^2P_{3/2}$) is produced by collisional excitation transfer of $O_2(^1\Delta)$ to I_2 and I. Plasma production of $O_2(^1\Delta)$ in electrical COILs (eCOILs) eliminates liquid phase generators. For the flowing plasmas used for eCOILs (He/O_2, a few to tens of torr), self-sustaining electron temperatures, T_e, are 2–3 eV whereas excitation of $O_2(^1\Delta)$ optimizes with $T_e = 1-1.5$ eV. One method to increase $O_2(^1\Delta)$ production is by lowering the average value of T_e using spiker-sustainer (SS) excitation where a high power pulse (spiker) is followed by a lower power period (sustainer). Excess ionization produced by the spiker enables the sustainer to operate with a lower T_e. Previous investigations suggested that SS techniques can significantly raise yields of $O_2(^1\Delta)$. In this paper, we report on the results from a two-dimensional computational investigation of radio frequency (rf) excited flowing He/O_2 plasmas with emphasis on SS excitation. We found that the efficiency of SS methods generally increase with increasing frequency by producing a higher electron density, lower T_e, and, as a consequence, a more efficient production of $O_2(^1\Delta)$. © *2006 American Institute of Physics*. [DOI: 10.1063/1.2199387]

I. INTRODUCTION

Chemical oxygen iodine lasers are being investigated because of their optical fiber deliverable wavelength (1.315 μm), highly scalable continuous wave (cw) power, and favorable material interaction properties.[1–6] Operation of the chemical oxygen iodine laser (COIL) is based on an electronic transition between the spin-orbit levels of the ground state configuration of the iodine atom $I(^2P_{1/2}) \rightarrow I(^2P_{3/2})$ where the upper level is populated by near resonant energy transfer (quantum defect ~ 219 cm^{-1}) from $O_2(^1\Delta)$ to ground state $I(^2P_{3/2})$. The COIL generates ground state I by dissociative excitation transfer from $O_2(^1\Delta)$ to I_2.

Typically, $O_2(^1\Delta)$ is produced in an external chemical reactor by a gas-liquid reaction between gaseous chlorine and a basic hydrogen peroxide solution[7] producing yields approaching 100% of the oxygen emerging in the $O_2(^1\Delta)$ state. The long lifetime of $O_2(^1\Delta)$ (60 min) and robustness against quenching enables transport over long distances to the laser cavity. There are many system issues having to do with weight, safety, and the ability to rapidly modulate the production of the $O_2(^1\Delta)$ which have motivated investigations into methods to produce the precursor $O_2(^1\Delta)$ using flowing electric discharges and so produce a purely electrical excited laser (eCOIL).[8,9] Recent and ongoing investigations have shown that substantial yields of $O_2(^1\Delta)$ can be generated by an appropriately tailored electric discharge, typically in mixtures with rare gas diluents such as He.[10–22] Recently, positive gain was reported in atomic iodine resulting from electric discharge produced $O_2(^1\Delta)$,[23,24] followed by laser demonstrations.[25,26]

Much of the development of eCOIL has focused on efficiently generating $O_2(^1\Delta)$ by engineering the operating E/N (electric field/gas number density) of the discharge to be closer to the optimum value for exciting $O_2(^1\Delta)$. To maximize the fraction of discharge power that is directly dissipated in the electron-impact excitation of $O_2(^1\Delta)$, the electron temperature, T_e, should be near 1.2 eV, which corresponds to an E/N of ≈ 10 Townsend [1 Townsend (Td) $= 10^{-17}$ V cm^2]. Self-sustained discharges in He/O_2 mixtures operate at least a few tens of Td.[27]

One of the methods to reduce the time averaged electron temperature is to use a pulsed discharge analogous to that proposed in Refs. 12 and 17. In these devices a short, high power pulse (the spiker) is followed by a longer period of lower power (the sustainer) before applying another high power pulse. The duration of the high power pulse should be long enough for T_e to spike and for the gas to avalanche, producing an electron density in excess of the steady-state value. The high power pulse should be short enough so that the discharge does not come into a quasi-steady-state. If there is sufficient excess ionization during the period of lower power deposition, there may be an extended period where T_e falls below the self-sustaining value, T_{eo}, which for He/O_2 mixtures enables a more efficient production of $O_2(^1\Delta)$. The duty cycle of the spiker and the length of the sustainer should be chosen so that the average value of electron temperature $\bar{T}_e < T_{eo}$. The optimum length of the sus-

a)Electronic mail: natalie5@iastate.edu
b)Electronic mail: arakoni@uiuc.edu
c)Author to whom correspondence should be addressed; electronic mail: mjk@iastate.edu

tainer is then largely determined by the time required for the electron density to decrease to its steady-state value, thereby increasing T_e towards T_{eo}. This method for engineering T_e is often referred to as spiker-sustainer (SS) excitation.

In previous work, the scaling of production of $O_2(^1\Delta)$ was computationally investigated using global-kinetics[19] one-dimensional,[20] and two-dimensional models.[21] It was found that the yield of $O_2(^1\Delta)$ generally scaled linearly with energy deposition for moderate loadings (a few eV/O_2 molecule) up to 5–8 eV/molecule. Energy deposition beyond those values produced excess dissociation which ultimately reduced yield. Initial scaling studies of SS excitation methods, discussed in Ref. 20, suggested that under ideal conditions, as are represented by global models, $O_2(^1\Delta)$ yields approaching 30% might be possible using SS methods. In this work, we computationally investigate SS methods for optimizing $O_2(^1\Delta)$ using a two-dimensional (2D) model that more realistically represents the electrical circuitry, electrode losses, uniformity and flow considerations. In particular, we investigated capacitively coupled radio frequency (rf) excited systems in He/O_2 mixtures. We found that SS methods do hold the potential for increasing $O_2(^1\Delta)$ yields above that for cw excitation for the same average power, though the amount of the increases is less than that suggested by the global models.

The model and reaction mechanism are briefly described in Sec. II. The results from our investigation are discussed in Sec. III where yields and efficiency of $O_2(^1\Delta)$ production are compared for cw and SS excitations for rf carrier frequencies of 13, 27, and 40 MHz. Optimization of $O_2(^1\Delta)$ production using the SS technique is discussed in Sec. IV. Concluding remarks are in Sec. V.

II. DESCRIPTION OF THE MODEL

The model used in this study, nonPDPSIM, is a multifluid 2D hydrodynamics simulation in which transport equations for all charged and neutral species and Poisson's equation are integrated as a function of time. nonPDPSIM is described in detail in Ref. 28. Poisson's equation [Eq. (1)], transport equations for conservation of the charged species [Eq. (2)], and the surface charge balance equation [Eq. (3)] are simultaneously integrated using a Newton iteration technique,

$$-\nabla\cdot(\varepsilon_0\varepsilon_r\nabla\Phi)=\sum_j N_j q_j+\rho_s, \tag{1}$$

$$\frac{\partial N_j}{\partial t}=-\nabla\cdot\mathbf{\Gamma}_j+S_j, \tag{2}$$

$$\frac{\partial\rho_s}{\partial t}=\sum_j q_j(-\nabla\cdot\mathbf{\Gamma}_j+S_j)-\nabla\cdot[\sigma(-\nabla\Phi)]. \tag{3}$$

Here ε_0, ε_r, Φ, ρ_s, N_j, $\mathbf{\Gamma}_j$, σ, S_j, and q_j are the permittivity of free space, dielectric constant, electric potential, surface charge density, conductivity of solid materials, sources, and charge, respectively. The subscripts j denote gas-phase species. Updates of the charged particle densities and electric potential are followed by an implicit update of the electron temperature by solving the electron energy equation for average energy ε,

$$\frac{\partial(n_e\varepsilon)}{\partial t}=q\mathbf{\Gamma}_e\cdot\mathbf{E}-n_e\sum_j N_j\kappa_j-\nabla\cdot\left(\frac{5}{2}\varepsilon\mathbf{\Gamma}_e-\lambda_e\nabla T_e\right), \tag{4}$$

where $\frac{3}{2}kT_e=\varepsilon$. The terms in Eq. (4) are for the contribution from Joule heating, summation of elastic and inelastic impact processes with heavy neutrals and ions with energy loss κ_j, and electron heat flux consisting of terms for electron energy flux (Γ_e) and a conduction (λ_e is the electron thermal conductivity). The electron transport coefficients and rate coefficients for bulk electrons as a function of T_e are obtained by solving the zero-dimensional Boltzmann's equation for the electron energy distribution to capture the non-Maxwellian nature of the electron swarm. These values are stored in a tabular form and interpolated during execution of the code. The tables are periodically updated to reflect changes in species densities. These updates are then followed, in a time splicing manner, with an implicit update of neutral particle densities.

The fluid averaged advective velocity $\mathbf{v}$ is obtained by solving a modified form of the compressible Navier-Stokes equations in which momentum transfer from ion and electron collisions and acceleration by the electric field are included in the momentum equation, and Joule heating is included in the energy equations,

$$\frac{\partial\rho}{\partial t}=-\nabla\cdot(\rho\mathbf{v})+(\text{inlets, pumps}), \tag{5}$$

$$\frac{\partial(\rho\mathbf{v})}{\partial t}=-\nabla p-\nabla\cdot(\rho\mathbf{v}\mathbf{v})-\nabla\cdot\boldsymbol{\tau}+\sum_j(q_jN_j-M_j\mu_jS_j)\mathbf{E}, \tag{6}$$

$$\frac{\partial(\rho c_pT)}{\partial t}=-\nabla(-\kappa\nabla T+\rho\mathbf{v}c_pT)+\sum_j\mathbf{j}_j\cdot\mathbf{E}-\sum_i R_i\Delta H_i+p\nabla\cdot\mathbf{v}. \tag{7}$$

Here ρ is the total mass density, p is the thermodynamic pressure, $\boldsymbol{\tau}$ is the viscosity tensor, c_p is the heat capacity, κ is the species averaged thermal conductivity, μ is the mobility, and M the molecular weight. The subscripts j are for summations over species. ΔH_i is the change in enthalpy due to reaction i having total rate R_i. The reactions include Frank-Condon heating from electron-impact dissociation of molecules as well as conventional chemical reactions. The sums (other than for reactions) are over all charged and neutral species. The contributions to momentum from charged particles include those of electrons. The contributions to the energy equation from Joule heating include contributions from ions. The heat transfer from electrons is included as a collisional change in enthalpy. The relationship among pressure, density, and temperature is given by the ideal-gas law. The contributions to momentum due to charged particle transport assume that the collision frequencies with electrons and ions are large compared to the time rate of change in the

electric field, and so there is little momentum that is instantaneously stored in the charged particles.[29]

The reaction mechanism for He/O_2 plasmas used here is essentially the same as that described in Refs. 19–21, and involves reactions in the gas-phase discharge and afterglow as well as recombination and quenching reactions on the discharge tube walls. The species in the model are ground state neutrals O_2, O, O_3, and He; vibrationally excited $O_2(v)$ (representing the total vibrational population consisting of the first four vibrational levels of O_2); electronic states $O_2(^1\Delta)$, $O_2(^1\Sigma)$, $O(^1D)$, $O(^1S)$, and $He(^2S)$; and ions O_2^+, O^+, O_2^-, O^-, O_3^-, and He^+.

The states of primary interest, the precursors to the eCOIL, are $O_2(^1\Delta)$ (0.97 eV) and $O_2(^1\Sigma)$ (1.6 eV), which are dominantly produced in the discharge region by direct electron impact with the ground state,

$$e + O_2 \rightarrow O_2(^1\Delta) + e, \tag{8}$$

$$e + O_2 \rightarrow O_2(^1\Sigma) + e. \tag{9}$$

Production of $O_2(^1\Sigma)$ generally also results in generation of $O_2(^1\Delta)$ through rapid collisional quenching reactions with atomic oxygen O. The atomic oxygen is dominantly produced by electron-impact dissociation of O_2,

$$e + O_2 \rightarrow O + O + e, \tag{10}$$

$$O + O_2(^1\Sigma) \rightarrow O + O_2(^1\Delta). \tag{11}$$

Note that the $O_2(^1\Sigma)$ and $O_2(^1\Delta)$ states have radiative lifetimes of 12 s and approximately 1 h. These states are only nominally quenched by collisions with species other than electrons for the conditions of interest although at higher pressures quenching of $O_2(^1\Delta)$ by O_3 becomes important. These electron collisions are, in order of importance, superelastic relaxation, dissociative excitation, and ionization. Other channels for $O_2(^1\Sigma)$ production (although less important for the conditions of interest) are through production and quenching of $O(^1D)$,

$$e + O_2 \rightarrow O(^1D) + O + e, \tag{12}$$

$$e + O \rightarrow O(^1D) + e, \tag{13}$$

$$O(^1D) + O_2 \rightarrow O + O_2(^1\Sigma). \tag{14}$$

The generation of $O_2(^1\Sigma)$ in these reactions is then followed by quenching by O to $O_2(^1\Delta)$. As the density of $O_2(^1\Delta)$ increases to the many percent level, losses to upper electronic states, superelastic deexcitation to the ground state, and dissociation begin to become important.

$$e + O_2(^1\Delta) \rightarrow O_2(^1\Sigma) + e, \tag{15}$$

$$e + O_2(^1\Delta) \rightarrow O_2 + e, \tag{16}$$

$$e + O_2(^1\Delta) \rightarrow O + O + e, \tag{17}$$

$$e + O_2(^1\Delta) \rightarrow O(^1D) + O + e. \tag{18}$$

The $O_2(^1\Delta)$ then persists far into the afterglow due to its long radiative lifetime, where the most significant quenching mechanism is through collisions with O atoms,

$$O + O_2(^1\Delta) \rightarrow O_2 + O. \tag{19}$$

At this point energy pooling and quenching reactions with $O_2(^1\Delta)$ and O_3 also begin to reduce $O_2(^1\Delta)$ yields, though not significantly for our conditions. The rate of quenching $O_2(^1\Delta)$ by collisions with the walls is uncertain due to the variability of the quenching probability with temperature and conditions of the wall. Based on estimates for similar conditions, we have assigned a wall quenching coefficient of 10^{-5}, which is insignificant for typical eCOIL conditions.

The effective yield of $O_2(^1\Delta)$ is defined as the ratio of the combined $O_2(^1\Delta)$ and $O_2(^1\Sigma)$ densities to the sum of the densities of all oxygen-containing species on a molecular O_2 basis,

$$Y = \frac{[O_2(^1\Delta) + O_2(^1\Sigma)]}{\{[O_2] + [O_2(^1\Delta)] + [O_2(^1\Sigma)] + 0.5[O] + 1.5[O_3]\}}. \tag{20}$$

This choice of yield was made with the prior knowledge that the majority of $O_2(^1\Sigma)$ is quenched directly to $O_2(^1\Delta)$. As such, Eq. (20) is the most relevant for the best case energy scaling.

III. CONTINUOUS WAVE AND SPIKER-SUSTAINER EXCITATIONS

A schematic of the idealized eCOIL device we modeled is shown in Fig. 1. A $He/O_2=70/30$ mixture is flowed through a quartz tube 60 cm in length and 6 cm in diameter at 3 Torr. A rf electric discharge is operated between two ring electrodes 2 cm wide with centers separated by 13 cm. The electrodes are powered up to a few hundred watts at 13.56, 27, or 40 MHz. The flow rate of 6 lpm corresponds to an average axial inlet speed of 985 cm/s. Our investigations were limited to the region of the reactor prior to supersonic expansion and injection of I_2. The numerical grid uses an unstructured, cylindrically symmetric mesh with triangular elements. The wall temperature was held fixed at 300 K assuming active water-jacket cooling (not included in the mesh).

A. Continuous wave excitation

As a point of departure and to provide a basis of comparison, $O_2(^1\Delta)$ production in a flowing afterglow using cw rf capacitive excitation will be discussed. The base case operating conditions are $He/O_2=70/30$, 3 Torr, flow rate of 6 lpm, inlet gas temperature of 300 K, and power deposition of 40 W with a rf of 13.56 MHz.

Power deposition, electron temperature (T_e), and electron density (n_e) for the base case are shown in Fig. 2(a). Values are shown averaged over the rf cycle. Power deposition is peaked just off axis with a maximum of 0.2 W/cm^3. The peak value of T_e of 2.9 eV is near the upstream electrode where the electron density is low. T_e drops to 2.2 eV where the electron density is maximum at about 9.8×10^9 cm^{-3} and where the majority of the $O_2(^1\Delta)$ is produced. The region of elevated T_e extends significantly beyond the rf electrodes

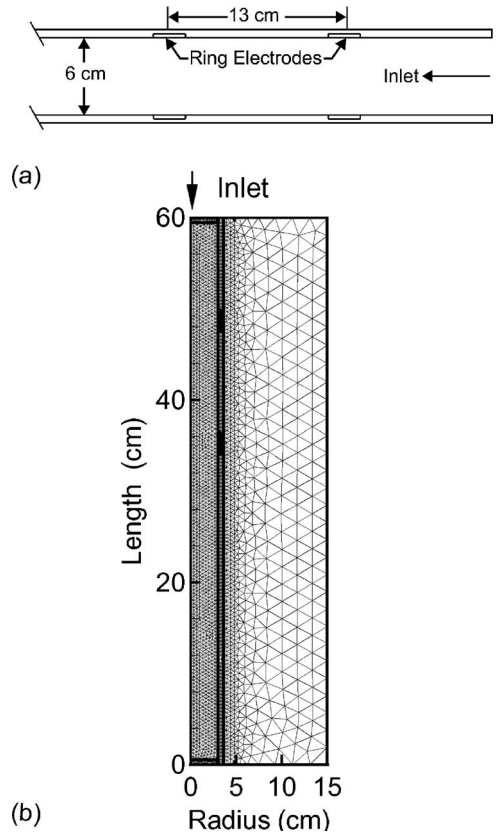

FIG. 1. Schematic of the cylindrical discharge tube. (a) Close-up showing ring electrodes and (b) complete computational domain showing the numerical mesh. The flow enters uniformly from the right (or top) where pressure, speed, and temperature are specified. The walls are held at constant temperature and mass flux is conserved at the outlet. Boundary conditions for solution of Poisson's equation require the extension of computational domain beyond the tube.

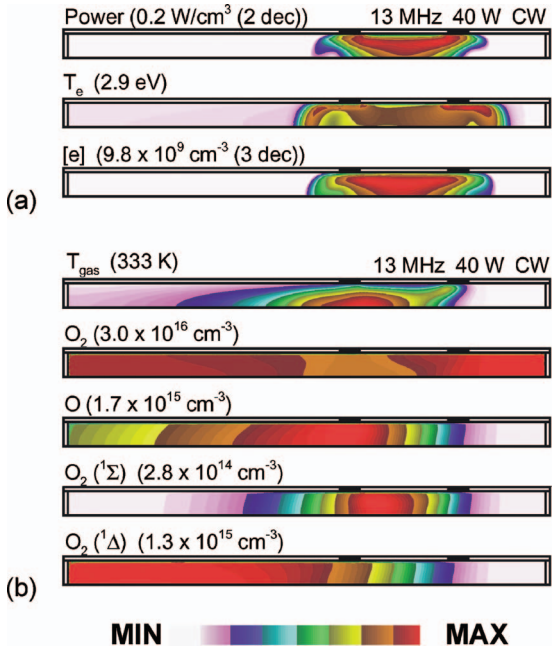

FIG. 2. (Color) Plasma properties and species densities for the base case conditions ($He/O_2=70/30$, 3 Torr, 6 lpm, 40 W) when using cw excitation at 13.56 MHz. (a) Power deposition, electron temperature, and electron densities; and (b) gas temperature and densities of O_2, O, $O_2(^1\Sigma)$, and $O_2(^1\Delta)$. All values are averaged over one rf period. The flow is from the right. The scales are linear with zero minimum values with the exception of T_{gas} unless the number of decades (i.e., "decs") is indicated for log plots. The maximum value is indicated in each figure. Depletion in ground state O_2 is due to gas heating by the localized power deposition. $O_2(^1\Delta)$ maximizes downstream in part due to quenching of $O_2(^1\Sigma)$.

(upstream and downstream) due to the large electron thermal conductivity and gas flow which entrains ions through their large momentum transfer. Although the electrons transfer little momentum to or from the gas, the electrons are pulled by the ions in the downstream direction through the ambipolar electric field. The electron density is as large as 10^9 cm^{-3}, a few centimeters ahead of the upstream electrode due to thermal conduction and diffusion of electrons against the advective flow and some local ionization. The steep rise in electron density at this point marks the front end of the reactive plasma zone. The same action occurs on the downstream side of the discharge. With diffusion now in the direction of the advective flow, the length of the afterglow is extended. The downstream extension of the plasma zone is aided by rarefaction of the gas downstream of the electrodes that provides for more rapid charge particle diffusion, and dissociation of O_2 that reduces the rate of loss of electrons by dissociative attachment.

Gas temperature, T_g, and densities of O_2, O, $O_2(^1\Sigma)$, and $O_2(^1\Delta)$ are shown in Fig. 2(b) for the base case. T_g increases by 33 K above ambient by Joule and Frank-Condon heating. The peak in the gas temperature is shifted downstream by the gas flow. Heating occurs primarily near the electrodes where the electric field is largest (see the local peak in T_g near the upstream electrode) and secondarily off axis in the bulk plasma where the ion density is largest. Thermal conduction and heat transfer at the walls shift the peak in T_g to the center of the tube. The gas returns to near ambient values at the exit.

Dissociation and excitation processes contribute to depletion of ground state O_2 in addition to that due to rarefaction by gas heating. Electron-impact dissociation produces about 6% of the depletion with an additional 5% coming from electron-impact excitation to $O_2(^1\Delta)$ and $O_2(^1\Sigma)$. The density of O atoms peaks 26 cm downstream, decreasing thereafter due to recombination on the walls, and three-body association reactions in the gas phase to form O_2 and O_3. The density of $O_2(^1\Sigma)$ peaks in the plasma zone where production is largest. As the density of O atoms increases, $O_2(^1\Sigma)$ is rapidly quenched to $O_2(^1\Delta)$ by collisions with O atoms in the flow direction after the discharge. After the $O_2(^1\Sigma)$ is converted to $O_2(^1\Delta)$, the density of $O_2(^1\Delta)$ only moderately decreases along the tube due to quenching. Excited states of O_2 and atomic O also extend 5–10 cm upstream of the electrodes, a consequence of the plasma extending upstream and back diffusion against the flow.

The combined yields of $O_2(^1\Delta)$ and $O_2(^1\Sigma)$ on axis for cw excitation are shown in Fig. 3 for different powers but for otherwise the base case conditions. The yield is maximum at the edge of the plasma zone near the downstream electrode. The yield is nearly constant thereafter, only slowly decreasing due to heavy particle quenching. Yields increase linearly with lower power deposition and begin to saturate at high powers. This is due to increased power losses to the elec-

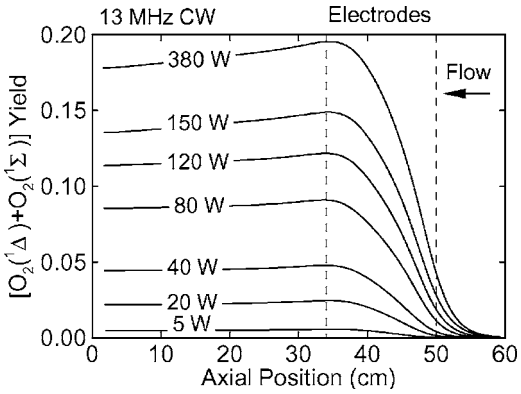

FIG. 3. Combined yield of $O_2(^1\Delta)$ and $O_2(^1\Sigma)$ along the axis of the tube ($He/O_2=70/30$, 3 Torr, 6 lpm) at 13.56 MHz for different powers. The flow is from the right. Maximum yields occur within the range of the electrodes. Yields scale linearly with lower power deposition and begin to saturate at high powers.

trodes, principally ion acceleration, typical for capacitive discharges. For example, for 40 W (specific energy deposition of 0.31 eV/O_2), the yield is about 4.5% at the exit of the tube or an efficiency of 0.15 $O_2(^1\Delta)$ molecules/eV of energy deposition. For 340 W (specific energy deposition of 2.95 eV/O_2), the yield is 19.5% at the end of the plasma zone and 18% at the exit of the tube, an efficiency of 0.04 $O_2(^1\Delta)$ molecules/eV.

B. Spiker-sustainer excitation

cw self-sustained discharges require that the sources of ionization and charged particle loss be equal. For moderate pressure mixtures of He/O_2, this translates into a balance between electron-impact ionization and electron loss by dissociative attachment to O_2 which requires $T_e=2-3$ eV. Unfortunately, the value of T_e at which power dissipation into excitation of $O_2(^1\Delta)$ and $O_2(^1\Sigma)$ is maximum is about 1–1.5 eV. This value is largely independent of gas mixtures as it is determined by the values of the excitation cross sections. As such, significant efforts have been expended in using gas additives to lower the E/N of the discharge so that T_e is 1–1.5 eV. In most cases, these values are inaccessible to self-sustained electric discharges. In SS systems for eCOIL applications, the discharge parameters are selected so that a significant fraction of the power deposition occurs at T_e below self-sustaining so that the rates of direct electron-impact excitation of $O_2(^1\Delta)$ and $O_2(^1\Sigma)$ are maximized.

Lowering the time averaged T_e to match the cross sections of desired excited states is a well known strategy. For example, externally sustained electric discharges, such as electron beam sustained discharges (EBSDs), have long been used to excite CO_2 lasers in $He/N_2/CO_2$ mixtures.[30] The self-sustaining E/N and T_e of these mixtures typically exceed that which optimizes excitation into the upper laser level, either by direct electron-impact vibrational excitation of CO_2 or through excitation transfer from $N_2(v=1)$. The external ionization provided by the electron beam enables the E/N provided by the discharge, for a given power deposition, to be below the self-sustaining value and be a better match to vibrational excitation of CO_2 and N_2. The disadvantage of this approach is the added complication and expense of the electron beam hardware. EBSD production of $O_2(^1\Delta)$ was investigated by Ionin *et al.*[13]

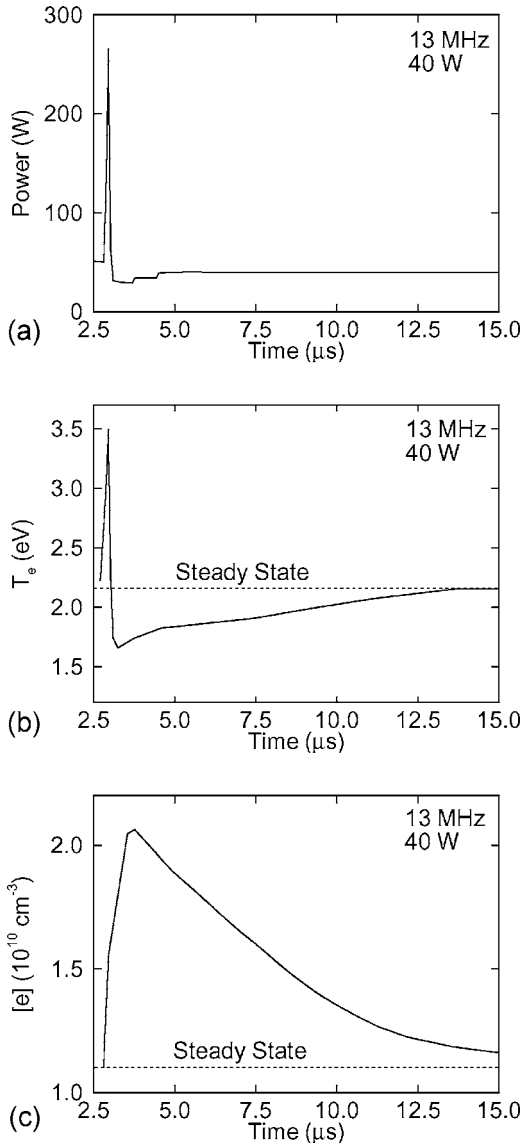

FIG. 4. Plasma properties when the He/O_2 gas mixture at 3 Torr is excited by a single spiker pulse. (a) Power deposition, (b) electron density, and (c) electron temperature. The excess electron density produced by the spiker enables the electron temperature to decrease to a more optimum value for excitation of $O_2(^1\Sigma)$. After the pulse the steady-state level is regained after 15–20 μs.

The SS technique attempts to achieve the same ends as the EBSD while using, in principle, a single discharge apparatus. Using the SS technique, the excess ionization provided by the spiker enables the E/N and T_e during the sustainer period, for a given time averaged power deposition, to be below self-sustaining similar to the EBSD. The excess ionization in the SS technique is provided *in situ* and, unlike the EBSD, is transient. That is, the discharge will eventually recover to a steady, self-sustaining state having a larger T_e.

The SS method we are investigating consists of pulsed modulated rf excitation; a series of high power rf pulses followed by a period of lower power rf excitation. As a point of departure, plasma properties during a single spiker pulse fol-

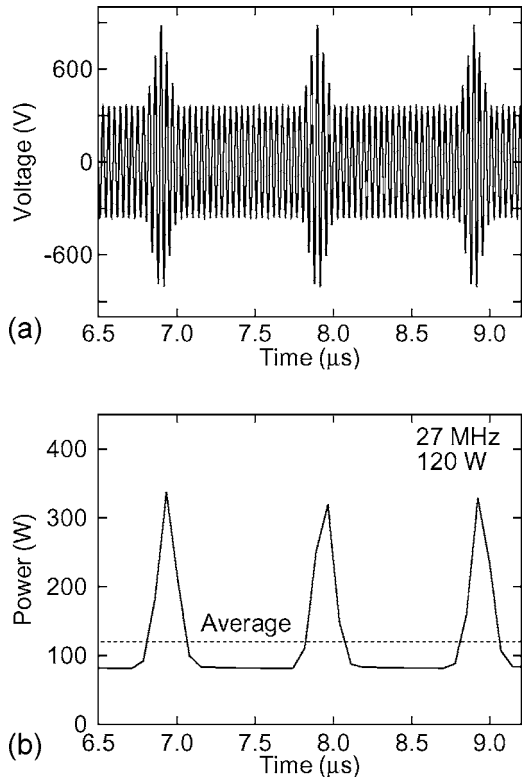

FIG. 5. Typical values of (a) voltage, and (b) power for SS excitation with 1 MHz repetition rate. The carrier frequency is 27 MHz. The V_{SS}/V_{cw} ratio is 5/2. Power is 120 W when averaged over a SS period (1 μs).

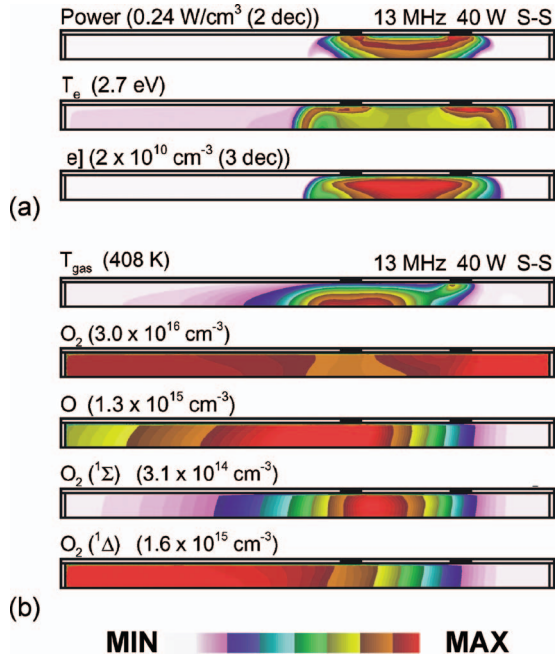

FIG. 6. (Color) Plasma properties and species densities for the base case conditions (He/O_2=70/30, 3 Torr, 6 lpm, 40 W) when using SS excitation at 13.56 MHz with a duty cycle of 20%. (a) Power deposition, electron temperature, and electron density; and (b) gas temperature and densities of O_2, O, $O_2(^1\Sigma)$, and $O_2(^1\Delta)$. All values are averaged over one SS period. Labeling is the same as in Fig. 2. The flow is from the right. With SS excitation the electron temperature is lower and maximum electron density higher compared with cw excitation.

lowed by a long sustainer period will be described. Using the base case conditions, the discharge, which is first operated in a steady state at 40 W, is then excited by a single short high power pulse of 270 W of duration of 200 ns and is then followed by a (sustainer) period of 40 W. The resulting power, and n_e and T_e on axis midway between the electrodes (approximately at the peak plasma density) are shown in Fig. 4 as a function of time. The spiker pulse avalanches n_e to values as high as 2.1×10^{10} cm^{-3} above the steady-state value of $n_{eo}=1.1\times10^{10}$ cm^{-3}. As recombination and attachment consume the excess ionization, n_e decreases towards n_{eo} over a period of 15–20 μs. The quasi-steady-state electron temperature is $T_{eo}=2.1$ eV. T_e increases during the spiker to avalanche the gas, thereby creating excess ionization and then decreases below T_{eo} after the spiker pulse terminates. As long as n_e is above n_{eo} then T_e is below T_{eo}, falling to as low as 1.6 eV. As the electron density decays towards n_{eo}, then T_e increases towards T_{eo}. These lower values of T_e, coupled with the excess ionization, have the potential to increase the production of $O_2(^1\Delta)$.

Typical voltage and power wave forms for a discharge operating in a SS mode for a time averaged power of 120 W are shown in Fig. 5. The conditions are otherwise the same as the base case. Excess ionization is provided by means of a high voltage spiker pulse (V_{SS}) of 200 ns duration repeated at 1 MHz at the carrier frequency of 27 MHz yielding a duty cycle of 20%. In between the spiker pulses, the plasma is sustained by a cw rf voltage (V_{cw}). The choices of V_{SS}/V_{cw} =5/2 and the triangular spiker pulse shape are somewhat arbitrary and have not been optimized for maximum yield of $O_2(^1\Delta)$. Power is averaged over the full SS period of 1 μs and the voltages V_{SS} and V_{cw} are adjusted to maintain the total time averaged power deposition at the specified value. Typically up to 15—20 (15–20 μs) of SS periods were simulated in order for the system to come into a pulse-periodic steady state. For the results in Fig. 5 (time averaged power of 120 W) the power during the spiker reaches 320 W with a peak $V_{SS}=900$ V resulting in the power during the sustainer being approximately 90 W with $V_{cw}=360$ V.

Time averaged plasma properties and species densities for the base case conditions when using SS (duty cycle 20%, $V_{SS}/V_{cw}=5/2$, 1 MHz repetition rate, and 13.56 MHz carrier frequency) are shown in Fig. 6 for 40 W average power. Values have been averaged over the entire 1 μs SS period. (Compare these results to Fig. 2 for cw excitation.) With SS excitation, the time averaged T_e is lower in the volume where the electron density is maximum while the time averaged n_e is larger. With SS excitation, the time averaged $T_e=1.7$ eV where n_e is maximum whereas with cw excitation, T_e =2.2 eV. The T_e remains near its cw value adjacent to the electrodes where sheath heating dominates. The time averaged maximum value of n_e increases from 9.8×10^9 cm with cw excitation to 2×10^{10} cm^{-3} with SS excitation. The decrease in T_e and increase in n_e are both favorable for more efficient $O_2(^1\Delta)$ production. The relative spatial distributions of species densities [O, O_2, $O_2(^1\Delta)$, and $O_2(^1\Sigma)$] do not significantly differ from the cw case. The exception is the spatial distribution of T_g that has more localized heating at the electrodes.

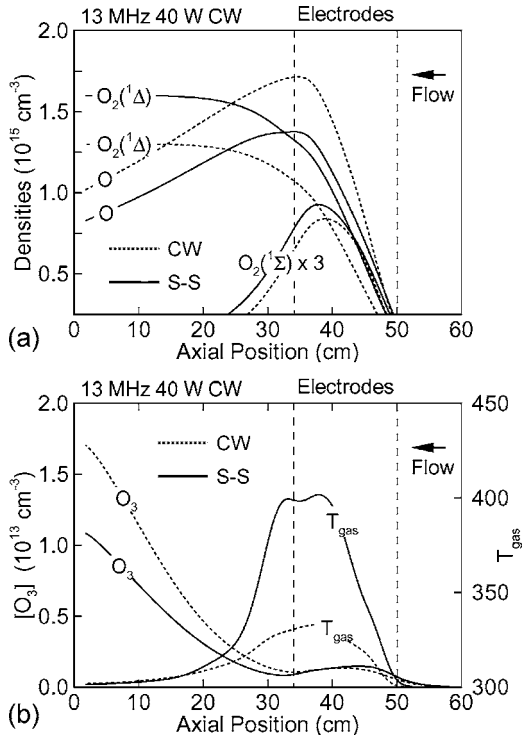

FIG. 7. Oxygen atomic and molecular densities (a) and gas temperature (b) along the axis for the base case conditions ($He/O_2=70/30$, 3 Torr, 6 lpm, 40 W) when using cw (dotted line) and SS (solid line) excitations. The flow is from the right. The degree of dissociation decreases and $O_2(^1\Delta)$ production increases with SS excitation.

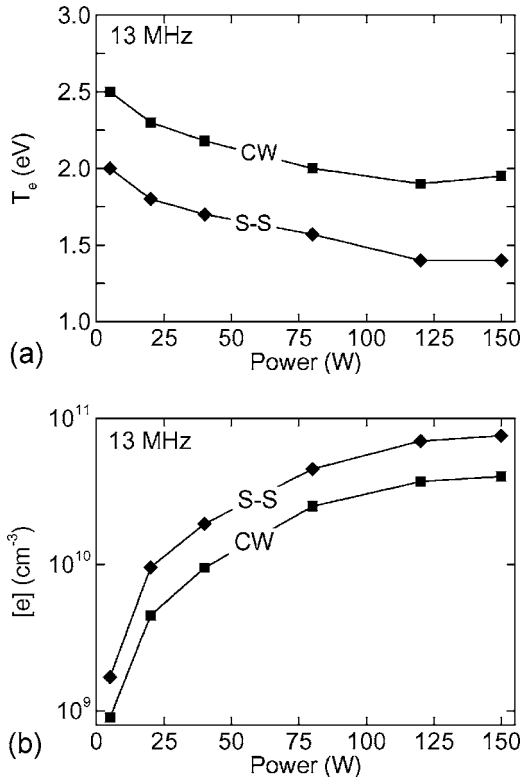

FIG. 8. Plasma parameters as a function of power for cw and SS excitations. (a) Electron temperature and (b) peak electron density. The electron temperature is measured at the location of peak electron density. The values are averaged over a SS period of 1 μs.

Time averaged species densities and gas temperature on the axis of the tube are compared for cw and SS excitations in Fig. 7. With SS excitation, the lower value of T_e results in less electron-impact dissociation of O_2, producing a smaller density of O atoms, while increasing the rate of excitation $O_2(^1\Delta)$. The contribution of quenching of $O_2(^1\Sigma)$ to production of $O_2(^1\Delta)$ by collisions with O atoms is about 20%. This quenching is somewhat more rapid in the cw case due to the larger density of O atoms. The production of O_3 is also larger in the cw case due to the larger production of O atoms, as shown in Fig. 7(b). The peak gas temperature is 400 K with SS excitation, whereas with cw excitation the peak T_g is only about 333 K. This is counterintuitive as the smaller amount of Frank-Condon heating due to there being less dissociation with SS excitation should produce a lower T_g. The larger time averaged value of n_e and lower value T_e obtained with SS excitation produce more vibrationally excited O_2 that undergoes V-T relaxation and more charge exchange heating. As a result, T_g increases with SS excitation.

The time averaged n_e and T_e at the location of the maximum electron density are shown in Fig. 8 as a function of power for cw and SS excitations. For powers between 10 and 150 W, T_e is approximately 0.5 eV lower with SS excitation compared to cw excitation, while the electron density is approximately a factor of 2 larger. Note that with increases in power, T_e decreases for both cw and SS excitations. This results from the larger degree of dissociation of O_2 and larger density of excited states. The larger dissociation of O_2 results in there being less dissociative attachment and fewer electron losses, and so a smaller T_e is required to sustain the discharge. The larger excited state densities enable a larger rate of multistep ionization which also allows for a smaller value of T_e.

Atomic oxygen and $O_2(^1\Delta)$ densities on axis for 40 and 120 W are shown in Fig. 9. The exit density of $O_2(^1\Delta)$ increases with SS compared to cw excitation whereas the O atom density decreases. The location of the maximum O atom density progressively moves downstream with increasing power due in large part to the increasing gas temperature, rarefaction, and extension of the plasma zone.

The combined yields of $O_2(^1\Delta)$ and $O_2(^1\Sigma)$ along the axis and at the exit of the tube for cw and SS excitations for different powers are shown in Fig. 10. The efficiency of production of $O_2(^1\Delta)$, molecules/eV of energy deposition, is also shown. For these discharge parameters, yields are typically higher for SS excitation for low powers and converge at higher powers (150 W). For example, at low power (20 W) the energy deposition required to produce one $O_2(^1\Delta)$ molecule is 7.3 eV for cw and 5.6 eV for SS excitation, netting a 30% improvement in $O_2(^1\Delta)$ yield. This improvement in yield diminishes as the total power is increased until, for these conditions, the advantage of SS excitation is lost for a power of 120 W. The decrease in improvement using the SS is likely the natural decrease in T_e that occurs when increasing power with cw excitation, as shown in Fig. 8. As T_e decreases towards 1 eV, the improvement in efficiency of exciting $O_2(^1\Delta)$ obtained by lowering T_e another 0.5 eV with SS excitation is diminished.

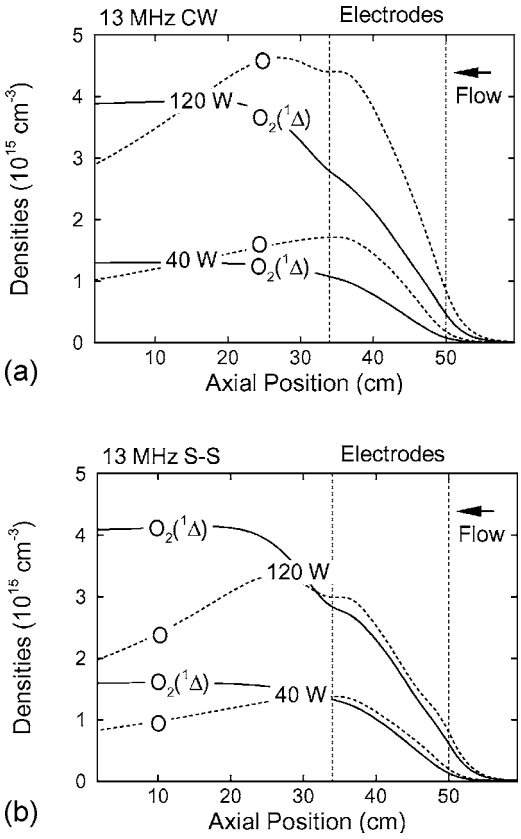

FIG. 9. Atomic oxygen and $O_2(^1\Delta)$ along the axis for 40 and 120 W. (a) cw and (b) SS. The flow is from the right. Dissociation of O_2 is significantly suppressed with SS excitation.

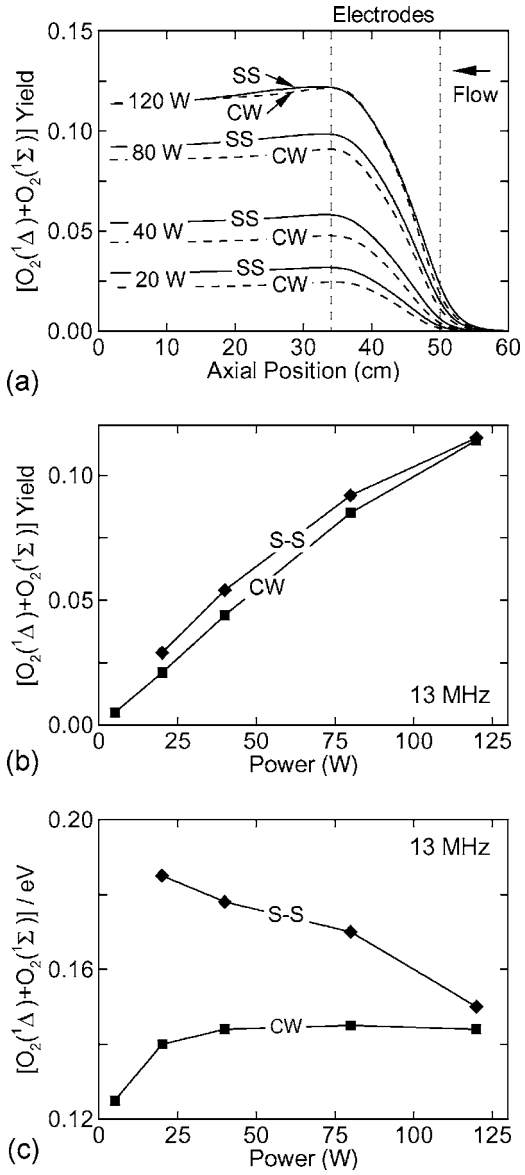

FIG. 10. Plasma parameters as a function of power for cw and SS excitations at 13.56 MHz. ($He/O_2=70/30$, 3 Torr, 6 lpm). (a) Combined yield of $O_2(^1\Delta)$ and $O_2(^1\Sigma)$ along the axis for flow from the right, (b) combined yields at the outlet of the tube, and (c) efficiency of $O_2(^1\Delta)$ production. Yields are typically higher for SS regime for low power but approach cw excitation at high powers.

The choice of carrier frequency is important due to the dependence of ionization rate and T_e on frequency. For example, the combined yields of $O_2(^1\Delta)$ and $O_2(^1\Sigma)$ along the axis, exit yield, and efficiency for a carrier frequency of 27 MHz using cw and SS excitations are shown in Fig. 11 for different powers. As with 13.56 MHz, yields are typically higher for SS compared to cw excitation at low powers. The efficiency obtained with two methods also converges at high powers. At 20 W, the energy deposition required to produce an $O_2(^1\Delta)$ molecule with SS excitation decreases to 4.6 eV at 27 MHz. This enables a 42% improvement in efficiency compared to cw excitation, while at 13.56 MHz, the improvement is 30% for the same conditions.

$O_2(^1\Delta)$ production efficiency increases with increasing carrier frequency with cw excitation as well. For example, $O_2(^1\Delta)$ production efficiency as a function of power with cw excitation for 13.56 and 27 MHz is shown in Fig. 12(a). The efficiency is larger at 27 MHz for powers up to 150 W. At both frequencies, efficiency first increases with power and then saturates. The increase with power results from the decrease in T_e (more dissociation of O_2 and less dissociative attachment) that enables better matching with cross section for excitation of $O_2(^1\Delta)$. This advantage is offset by the dissociation of O_2 and rarefaction that occurs at higher power. Although increasing frequency also increases the efficiency of excitation with SS excitation, the trend with power is opposite to that with cw excitation, as shown in Fig. 12(b). Since T_e is already low [and near optimum for $O_2(^1\Delta)$ production] with SS excitation, the decrease in O_2 density that results from electron-impact dissociation with increasing power serves to lower the fractional power expended in $O_2(^1\Delta)$ excitation.

The scaling of yield with carrier frequency depends on the method of excitation, as shown in Fig. 13(a). When increasing frequency, T_e generally decreases due to the more efficient electron ionization and reduction in power loss to ion acceleration that occurs at higher frequencies, as shown in Fig. 13(b). With cw excitation, the decrease of T_e with increasing frequency up to 40 MHz brings T_e closer to the optimum range of 1–1.5 eV. As a result, the yield of $O_2(^1\Delta)$ monotonically increases attaining a maximum at about 33 MHz. With SS excitation, T_e is lower than with cw power and near the optimum value at 27 MHz. Increasing fre-

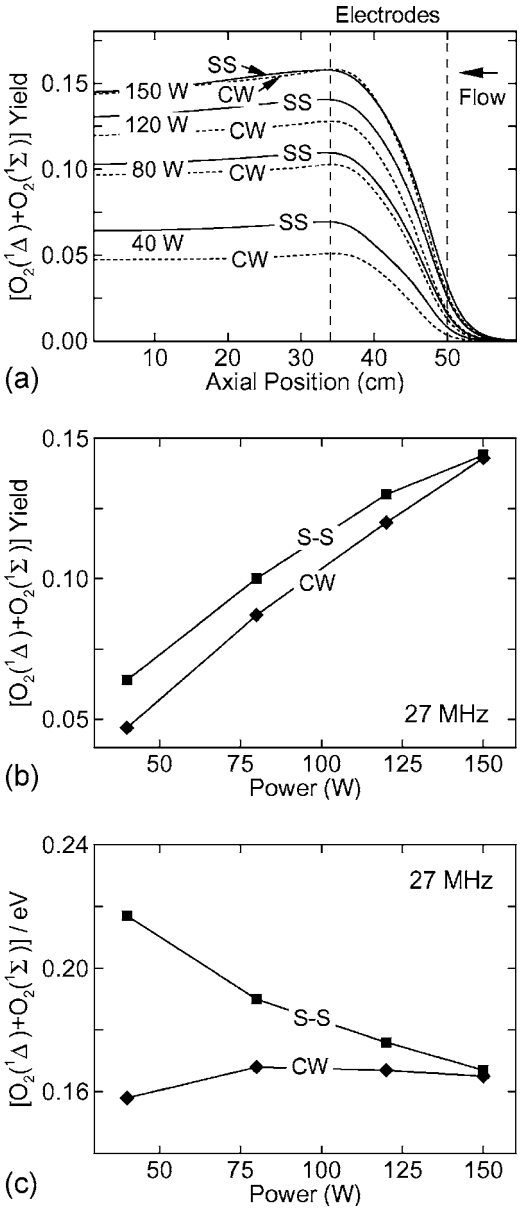

FIG. 11. Plasma parameters as a function of power for cw and SS excitations at 27 MHz. ($He/O_2=70/30$, 3 Torr, 6 lpm). (a) Combined yield of $O_2(^1\Delta)$ and $O_2(^1\Sigma)$ along the axis for flow from the right, (b) combined yields at the outlet of the tube, and (c) efficiency of $O_2(^1\Delta)$ production.

quency from 13.56 to 27 MHz decreases T_e into the optimum range producing an increase in yield. Further increases in frequency decrease T_e to being below optimum for $O_2(^1\Delta)$ production and so yield decreases.

IV. OPTIMIZING SS EXCITATION

Optimizing $O_2(^1\Delta)$ yield using SS excitation depends upon the plasma dynamics that result from the details of the pulse shape, as shown in Fig. 14(a). These characteristics include the carrier frequency, duty cycle (fraction of the SS cycle for the spiker), SS frequency (time between spiker pulses), spiker pulse shape, and value of V_{SS}/V_{cw}. For example, combined yields as function of V_{SS}/V_{cw} are shown in Fig. 14(b). Maximum yields are obtained for $V_{SS}/V_{cw}=2.5-3$. $V_{SS}/V_{cw}=1$ corresponds to cw excitation. As

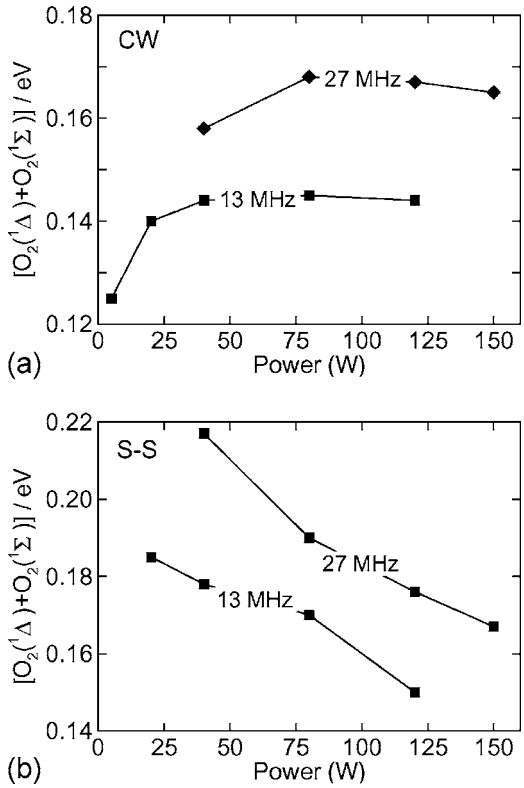

FIG. 12. Comparison of efficiency of $O_2(^1\Delta)$ production for 13.56 and 27 MHz with (a) cw and (b) SS excitations. Using higher carrier frequencies is favorable for both cw and SS excitations.

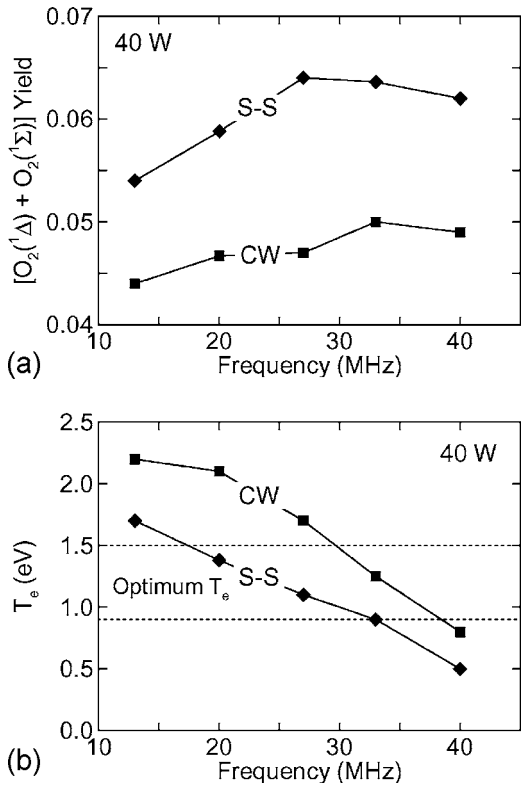

FIG. 13. Plasma parameters as a function of rf for cw and SS excitations. (a) Combined yield at the end of the tube and (b) electron temperature. Electron temperatures generally decrease with increasing carrier frequency and may become too low for optimum $O_2(^1\Delta)$ production.

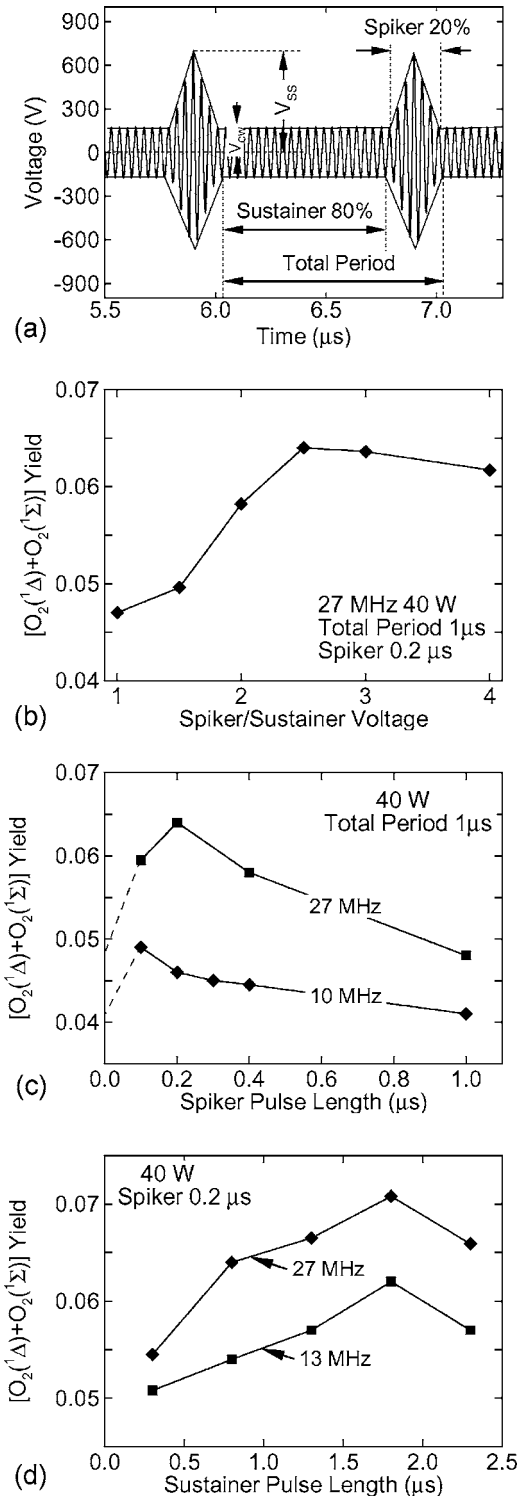

FIG. 14. Optimization of $O_2(^1\Delta)$ production with SS excitation. (a) Voltage wave form for a duty cycle of 20%. Combined yield as a function of (b) the ratio of spiker to sustainer voltage, (c) duty cycle for SS excitation at 10 and 27 MHz carrier frequencies, and (d) sustainer pulse length. Increasing the duty cycle generally decreases yield as the discharge appears to operate in a cw mode.

V_{SS}/V_{cw} increases from one, the amount of excess ionization increases, thereby enabling a lower value of T_e during the sustainer. When keeping the total power constant, as V_{SS}/V_{cw} increases a larger fraction of the power is expended during the avalanche when T_e is large and the efficiency of exciting $O_2(^1\Delta)$ is low. Therefore, very large values of V_{SS}/V_{cw} are not optimum. V_{SS}/V_{cw} should be large enough to produce sufficient excess ionization to last through the sustainer period, but small enough that the majority of the power is dissipated during the sustainer when T_e is low.

Combined yields as a function of spiker pulse length (duty cycle) for 10 and 27 MHz carrier frequencies are shown in Fig. 14(c) for a total SS period of 1 μs. Maximum yields are obtained for duty cycles of 10%–20% depending on carrier frequency. The ideal situation would be a delta-function spiker that produces a large electron temperature, efficiently creating large amounts of excess ionization and depositing little energy. The reality is that a finite time, even for large electron temperatures, is required to produce the excess ionization. For these conditions, that finite time is 100–200 ns. There are practical limitations for the length of the spiker since at least a rf cycle or two are required during the spiker. At 27 MHz and 20% duty cycle, there are five rf periods during the spiker, whereas at 10 MHz and 10% spiker duty cycle, there is only one rf period during the spiker. At the other extreme, as the duty cycle approaches unity SS excitation appears to be cw excitation as quasi-steady-state conditions are obtained during the spiker. Yield therefore decreases and approaches the cw value.

Increasing the sustainer pulse length from small values (<1 μs) increases $O_2(^1\Delta)$ production. For these conditions, $O_2(^1\Delta)$ yield optimizes for a sustainer pulse length of 1.8 μs, as shown in Fig. 14(d). The longer sustainer pulse enables a longer period of operating at low T_e. While keeping the total power constant, extending the sustainer reduces the amount of power dissipated during the spiker and so reduces the amount of excess ionization. With sufficient ionization during the spiker, the optimum sustainer length should approach the 10–15 μs typically required for the plasma to recover to a steady state.

Based on these and other scaling studies we find that $O_2(^1\Delta)$ production optimizes using SS techniques for the following conditions.

- Operate with a high carrier frequency to lower T_e and increase proportion of power dissipated by electrons.
- The spiker pulse length should be as short as possible while still providing sufficient excess ionization to last through the entire sustainer period.
- The spiker voltage should not elevate the electron temperature above that required for rapid ionization.
- The sustainer pulse length should be long enough that the majority of power is dissipated during the sustainer but not so long that the plasma fully recovers to its cw conditions.

V. CONCLUDING REMARKS

The consequences of spiker-sustain excitation on yield of $O_2(^1\Delta)$ in flowing He/O_2 plasmas were investigated with 2D plasma hydrodynamics model. SS techniques generally do lower the time averaged T_e compared to cw excitation and so improve the efficiency of excitation and yield for $O_2(^1\Delta)$. This advantage to SS excitation is diminished at higher powers where T_e is naturally lower for cw excitation. Lower duty

cycles (shorter spiker pulses) are generally more advantageous for SS excitation as the limit of a delta-function spiker is approached. Increasing the frequency of excitation is also advantageous due to the lowering of T_e and increase in n_e. Again, the advantage of SS excitation is diminished as frequency increases due to the natural decrease in T_e with cw excitation. The length of the sustainer pulse should be short enough so that T_e is largely below the self-sustaining value but long enough so that T_e and n_e begin recovering towards their steady-state values. This recovery indicates a good utilization of the excess ionization produced by the spiker.

ACKNOWLEDGMENTS

This work was supported by the Air Force Office of Scientific Research and the National Science Foundation (CTS-0520368).

[1]W. E. McDermott, N. R. Pchelkin, D. J. Benard, and R. R. Bousek, Appl. Phys. Lett. **32**, 469 (1978).
[2]H. Fujii, S. Yoshida, M. Iizuka, and T. Atsuta, J. Appl. Phys. **67**, 3948 (1990).
[3]A. Elior, B. D. Barmashenko, E. Lebiush, and S. Rosenwaks, Appl. Phys. B: Lasers Opt. **B61**, 37 (1995).
[4]M. Endo *et al.*, IEEE J. Quantum Electron. **34**, 393 (1998).
[5]D. Furman, E. Bruins, V. Rybalkin, B. D. Barmashenko, and S. Rosenwaks, IEEE J. Quantum Electron. **37**, 174 (2001).
[6]J. Kodymova, O. Spalek, V. Jirasek, M. Censky, and G. D. Hager, Appl. Phys. A: Mater. Sci. Process. **77**, 331 (2003).
[7]J. Kodymova and O. Spalek, Jpn. J. Appl. Phys., Part 1 **37**, 117 (1998).
[8]D. L. Carroll and W. C. Solomon, *ElectriCOIL: An Advanced Chemical Iodine Laser Concept, Proceedings of the XIII International Symposium on Gas Flow and Chemical Lasers and High Power Laser Conference, Florence, Italy, 18–22 September 2000*, edited by A. Lapucci (SPIE, Bellingham, WA, 2000), pp. 40–44.
[9]T. L. Henshaw, T. J. Madden, G. C. M. Il, B. T. Anderson, R. F. Tate, M. R. Berman, and G. D. Hager, AIAA Paper No. 2000-2424, 2000.
[10]D. L. Carroll, D. M. King, J. T. Verdeyen, B. Woodard, J. W. Zimmerman, L. Skorski, and W. C. Solomon, AIAA Paper No. 2003-4029, 2003.
[11]J. Schmiedberger, S. Hirahara, Y. Ichinoche, M. Suzuki, W. Masuda, Y. Kihara, E. Yoshitani, and H. Fujii, Proc. SPIE **4184**, 32 (2001).
[12]A. E. Hill, *The Next Generation of Controlled Avalanche Discharge Gas Lasers, International Conference on Lasers, Albuquerque, NM, 2000* (STS, McLean, VA, 2000).
[13]A. A. Ionin, Y. M. Klimachev, A. A. Kotkov, I. V. Kochetov, A. P. Napartovich, L. V. Seleznev, D. V. Sinitsyn, and G. D. Hager, J. Phys. D **36**, 982 (2003).
[14]T. V. Rakhimova *et al.*, AIAA Paper No. 2003-4306, 2003.
[15]Yu. V. Savin *et al.*, J. Phys. D **37**, 3121 (2004).
[16]A. N. Vasiljeva, K. S. Klopovskiy, A. S. Kovalev, D. V. Lopaev, Y. A. Mankelevich, N. A. Popov, A. T. Rakhimov, and T. V. Rakhimova, J. Phys. D **37**, 2455 (2004).
[17]A. Hicks, S. Norberg, P. Shawcross, W. Lempert, J. W. Rich, and I. Adamovich, J. Phys. D **38**, 3812 (2005).
[18]D. L. Carroll, J. T. Verdeyen, D. M. King, B. S. Woodard, L. W. Skorski, J. W. Zimmerman, and W. C. Solomon, IEEE J. Quantum Electron. **39**, 1150 (2003).
[19]D. S. Stafford and M. J. Kushner, J. Appl. Phys. **96**, 2451 (2004).
[20]D. S. Stafford and M. J. Kushner, J. Appl. Phys. **98**, 073303 (2005).
[21]R. Arakoni, D. S. Stafford, N. Yu. Babaeva, and M. J. Kushner, J. Appl. Phys. **98**, 073304 (2005).
[22]D. L. Carroll, J. T. Verdeyen, D. M. King, B. Woodard, L. Skorski, J. W. Zimmerman, and W. C. Solomon, *Recent Work on the Development of an Electric Discharge Oxygen Iodine Laser, XIV International Symposium on Gas Flow and Chemical Lasers and High Power Laser Conference, Wroclaw, Poland, 2002*, edited by K. Abramski, E. Plinski, and W. Wolinski (SPIE, Bellingham, 2002), pp. 316–326.
[23]D. L. Carroll *et al.*, Appl. Phys. Lett. **85**, 1320 (2004).
[24]D. L. Carroll *et al.*, IEEE J. Quantum Electron. **41**, 213 (2005).
[25]D. L. Carroll *et al.*, Appl. Phys. Lett. **86**, 111104 (2005).
[26]D. L. Carroll *et al.*, IEEE J. Quantum Electron. **41**, 1309 (2005).
[27]J. T. Verdeyen, D. M. King, D. L. Carroll, and W. C. Solomon, *Diagnostic Development for the ElectriCOIL Flow System, Proceedings of the Gas and Chemical Lasers and Intense Beam Applications III Conference, San Jose, CA, 22–24 January 2002*, edited by S. Davis and M. Heaven (SPIE, Bellingham, WA, 2002), pp. 154–160.
[28]M. J. Kushner, J. Phys. D **38**, 1633 (2005).
[29]C. C. Leiby and H. J. Oskam, Phys. Fluids **10**, 1993 (1967).
[30]M. J. Yoder, H. H. Legner, J. H. Jacob, and D. R. Ahouse, J. Appl. Phys. **49**, 3171 (1978).